

# Implementation of a Two-Equation $k-\omega$ Turbulence Model in NPARC

Dennis A. Yoder and Nicholas J. Georgiadis  
*Lewis Research Center*  
*Cleveland, Ohio*

Paul D. Orkwis  
*University of Cincinnati*  
*Cincinnati, Ohio*

Prepared for the  
34th Aerospace Sciences Meeting and Exhibit  
sponsored by the American Institute of Aeronautics and Astronautics  
Reno, Nevada, January 15-18, 1996



National Aeronautics and  
Space Administration

# IMPLEMENTATION OF A TWO-EQUATION $k-\omega$ TURBULENCE MODEL IN NPARC

Dennis A. Yoder,\* Nicholas J. Georgiadis\*  
National Aeronautics and Space Administration  
Lewis Research Center  
Cleveland, Ohio

and

Paul D. Orkwis\*  
University of Cincinnati  
Cincinnati, Ohio

## Abstract

The implementation of a two-equation  $k-\omega$  turbulence model into the NPARC flow solver is described. Motivation for the selection of this model is given, major code modifications are outlined, new inputs to the code are described, and results are presented for several validation cases: an incompressible flow over a smooth flat plate, a subsonic diffuser flow, and a shock-induced separated flow. Comparison of results with the  $k-\epsilon$  model indicate that the  $k-\omega$  model predicts simple flows equally well whereas, for adverse pressure gradient flows, the  $k-\omega$  model outperforms the other turbulence models in NPARC.

$P_t$	stagnation pressure
$R$	ratio of turbulent kinetic energy production to dissipation
$R_k, R_s, R_\omega$	$k-\omega$ turbulence model constants
$Re_t$	Reynolds number based on turbulent quantities
$Re_x$	Reynolds number based on axial position
$Re_\theta$	Reynolds number based on momentum thickness

## Symbols

$a$	speed of sound	$S_R$	surface roughness coefficient
$C_f$	skin friction coefficient along flat plate	$t$	time
$C_{\epsilon 1}, C_{\epsilon 2}$	$k-\epsilon$ turbulence model terms	$U_{\text{ref}(k-\epsilon)}$	reference velocity for turbulent kinetic energy limiter
$C_\mu$	$k-\epsilon$ turbulence model constant	$u$	velocity
$f_\mu, f_1, f_2$	$k-\epsilon$ turbulence model terms	$u_{cl}$	centerline velocity for Fraser diffuser
$H$	throat height of Sajben diffuser	$u_\tau$	friction velocity
$I$	turbulence intensity	$u_\infty$	free-stream velocity
$k$	turbulent kinetic energy	$u^+$	normalized velocity
$k_R$	average sand-grain surface roughness	$-\overline{uv}$	Reynolds stress
$M_t$	turbulent Mach number	$x, y$	Cartesian coordinates
$P$	static pressure	$y^+$	distance from wall normalized by shear length scale

\*AIAA member

$\alpha, \alpha_0, \alpha^*$	k- $\omega$ turbulence model constants
$\beta, \beta^*$	k- $\omega$ turbulence model constants
$\delta$	boundary layer thickness
$\epsilon$	rate of turbulent kinetic energy dissipation
$\mu$	dynamic viscosity
$\mu_t$	turbulent viscosity
$\mu_{t,max}$	maximum turbulent viscosity limiter
$\nu$	kinematic viscosity
$\Pi$	production term in k- $\epsilon$ model
$\rho$	density
$\sigma_k, \sigma_\epsilon, \sigma_\omega$	turbulent Prandtl numbers
$\omega$	specific turbulent kinetic energy dissipation rate
$\xi_k, \xi_\omega$	k- $\omega$ turbulence model terms
Subscripts:	
$i, j$	computational coordinates
max	maximum
min	minimum

### Introduction

In NASA's High Speed Research (HSR) program, computational fluid dynamics (CFD) is increasingly being used to design and evaluate inlet and nozzle configurations for High Speed Civil Transport (HSCT) applications. Accurately predicting flow separations and mixing between primary and secondary flows in highly turbulent mixer-ejector nozzles as well as pressure losses and bleed flows in supersonic mixed-compression inlets is a major challenge. The turbulence model employed is often the limiting factor in these types of simulations and, as a result, is often blamed for providing poor agreement with experimental data. Thus, the search for better models is ongoing.

Turbulence models vary from relatively simple algebraic models to one-equation, two-equation, and full Reynolds stress models. Moving to the next level of complexity

generally involves solving additional transport equations. Thus, as the model complexity increases, so does the effort required to implement the model. Higher level turbulence models are also more computationally expensive because they require more computer memory and cpu time. Two-equation models are commonly used because they are considered to provide relatively good results for the demand they place on computer resources.

The most widely used two-equation turbulence model, the k- $\epsilon$ , solves two transport equations for the turbulent kinetic energy  $k$  and the rate of dissipation of turbulent kinetic energy  $\epsilon$ . Important groundwork on this model was performed by Jones and Launder<sup>1</sup> and Launder and Spalding.<sup>2</sup> The Jones and Launder model is often referred to as the standard k- $\epsilon$  model.

The k- $\omega$  model is similar to the k- $\epsilon$  model except that the second turbulent quantity  $\omega$  is the *specific* dissipation rate (dissipation rate per unit turbulent kinetic energy). Kolmogorov<sup>3</sup> was the first to propose this type of model. Since then, others have made modifications to the original formulation. Among these are Menter<sup>4</sup> and Wilcox.<sup>5</sup> Wilcox<sup>6</sup> presents an interesting historical overview of the k- $\omega$  model.

Recent efforts at NASA Lewis Research Center to model the flow field inside subsonic diffusers have demonstrated the inability of current models to accurately predict flows with adverse pressure gradients. The k- $\omega$  model has been shown to predict separated flows better than the standard k- $\epsilon$  model, especially in flows with adverse pressure gradients.<sup>7,8</sup> As a result, the k- $\omega$  model of Wilcox<sup>5</sup> was recently installed in both the two- and three-dimensional versions of NPARC. Because the k- $\omega$  model is a two-equation model, it does not require additional cpu time relative to the k- $\epsilon$  model, and since it is similar in form to the k- $\epsilon$  model, a similar algorithm can be used. Furthermore, this model has the benefit of improved transition simulation and is capable of more realistic rough-wall treatments. This report provides an overview of some of the turbulence models already available in NPARC, a discussion of the implementation of the k- $\omega$  model in the code, and results obtained using the new model for several flow fields.

### NPARC Code

The NPARC code, previously known as the PARC code<sup>9</sup> and originally developed at the Arnold Engineering Development Center (AEDC), uses the Beam and Warming<sup>10</sup> approximate factorization algorithm to solve the Reynolds-averaged Navier-Stokes equations at discrete grid points. Generalized boundary conditions allow the user to specify any portion of a grid as a boundary. Noncontiguous multiple block interfacing can also be

used to simplify the grid generation of complex geometries. Cooper<sup>11</sup> discusses recent features of the code.

The NPARC code contains three algebraic turbulence models, the first of which is the Thomas model.<sup>12</sup> It computes turbulent viscosity for wall-bounded and free shear layer flows and has been optimized for the latter. The second, the Baldwin-Lomax model,<sup>13</sup> only computes turbulent viscosity in wall-bounded regions. An algebraic RNG (renormalized group theory) model<sup>14</sup> is also available.

NPARC also contains the Baldwin-Barth one-equation model<sup>15</sup> and a two-equation turbulence model based on the Chien low-Reynolds-number  $k$ - $\epsilon$  model,<sup>16</sup> which is presented below in detail to underscore its similarity to the  $k$ - $\omega$  model:

$$\mu_t = C_\mu f_\mu \rho \frac{k^2}{\epsilon} \quad (1)$$

$$\begin{aligned} \frac{\partial(\rho k)}{\partial t} + \frac{\partial(\rho u_i k)}{\partial x_i} &= \frac{\partial}{\partial x_i} \left[ \left( \mu + \frac{\mu_t}{\sigma_k} \right) \frac{\partial k}{\partial x_i} \right] \\ &+ \Pi - \rho \epsilon (1 + M_t^2) - 2\mu \frac{k}{y^2} \end{aligned} \quad (2)$$

$$\begin{aligned} \frac{\partial(\rho \epsilon)}{\partial t} + \frac{\partial(\rho u_i \epsilon)}{\partial x_i} &= \frac{\partial}{\partial x_i} \left[ \left( \mu + \frac{\mu_t}{\sigma_\epsilon} \right) \frac{\partial \epsilon}{\partial x_i} \right] \\ &+ C_{\epsilon 1} f_1 \Pi \frac{\epsilon}{k} - C_{\epsilon 2} f_2 \rho \frac{\epsilon^2}{k} - 2\mu \frac{\epsilon}{y^2} e^{(-0.5y^+)} \end{aligned} \quad (3)$$

where

$$\Pi = \mu_t \frac{\partial u_j}{\partial x_i} \left( \frac{\partial u_j}{\partial x_i} + \frac{\partial u_i}{\partial x_j} \right) \quad (4)$$

$$f_\mu = 1.0 - e^{(-0.0115y^+)} \quad (5)$$

$$f_1 = 1.0 \quad (6)$$

$$f_2 = 1.0 - 0.22e^{-(Re_t/6)^2} \quad (7)$$

$$Re_t = \frac{\rho k^2}{\mu \epsilon} \quad (8)$$

and  $C_\mu = 0.09$ ,  $C_{\epsilon 1} = 1.35$ ,  $C_{\epsilon 2} = 1.80$ ,  $\sigma_k = 1.0$ ,  $\sigma_\epsilon = 1.3$ . The turbulent Mach number is defined as  $M_t^2 = 2k/a^2$ , where  $a$  is the reference speed of sound, and is used in Sarkar's compressibility correction.<sup>17</sup> This compressibility correction has been incorporated into the NPARC code to compensate for the apparent increase in turbulent dissipation at higher Mach numbers. The  $\epsilon$ -equation (3) has been relatively insensitive to compressibility effects and therefore requires no modification.

The terms on the right-hand side of equations (2) and (3) correspond to the diffusion, production, dissipation, and near-wall damping terms, respectively. One of the difficulties with the  $k$ - $\epsilon$  model is that there is no natural boundary condition for  $\epsilon$  near a solid surface. Since the turbulent kinetic energy and the turbulent viscosity are both zero along a wall, the dissipation rate is set to zero as well. It is the near-wall damping terms of equations (2) and (3) that allow all the turbulent quantities to be set to zero near a viscous surface. Another problem with the Chien model is that it requires that the distance from the wall be calculated. In complicated geometries, and especially in three-dimensional cases, this can be difficult to compute. Lang and Shih<sup>18</sup> also point out that near-wall damping terms which use  $y^+$  are not desirable, particularly near separation regions.

The Wilcox  $k$ - $\omega$  model does not have the aforementioned shortcomings. The value of  $\omega$  near a viscous wall can be related to the surface roughness of the wall. This condition can be enforced at the boundary and does not require the use of near-wall terms or  $y^+$ . The Wilcox  $k$ - $\omega$  model is formulated as follows:

$$\mu_t = \alpha^* \frac{\rho k}{\omega} \quad (9)$$

$$\begin{aligned} \frac{\partial(\rho k)}{\partial t} + \frac{\partial(\rho u_i k)}{\partial x_i} &= \frac{\partial}{\partial x_i} \left[ \left( \mu + \frac{\mu_t}{\sigma_k} \right) \frac{\partial k}{\partial x_i} \right] \\ &+ \Pi - \beta^* \rho \omega k [1 + \xi_k F(M_t)] \end{aligned} \quad (10)$$

$$\begin{aligned} \frac{\partial(\rho \omega)}{\partial t} + \frac{\partial(\rho u_i \omega)}{\partial x_i} &= \frac{\partial}{\partial x_i} \left[ \left( \mu + \frac{\mu_t}{\sigma_\omega} \right) \frac{\partial \omega}{\partial x_i} \right] \\ &+ \alpha \frac{\omega}{k} \Pi - \rho \omega^2 [\beta + \beta^* \xi_\omega F(M_t)] \end{aligned} \quad (11)$$

where

$$\Pi = \mu_t \frac{\partial u_j}{\partial x_i} \left( \frac{\partial u_j}{\partial x_i} + \frac{\partial u_i}{\partial x_j} \right) \quad (12)$$

$$\alpha^* = \frac{\alpha_0^* + \left( \frac{Re_t}{R_k} \right)}{1 + \left( \frac{Re_t}{R_k} \right)} \quad (13)$$

$$\alpha = \frac{5}{9} \frac{\alpha_0 + \left( \frac{Re_t}{R_\omega} \right)}{1 + \left( \frac{Re_t}{R_\omega} \right)} (\alpha^*)^{-1} \quad (14)$$

$$\beta^* = \frac{9}{100} \frac{\frac{5}{18} + \left( \frac{Re_t}{R_s} \right)^4}{1 + \left( \frac{Re_t}{R_s} \right)^4} \quad (15)$$

$$\beta = \frac{3}{40} \quad (16)$$

$$Re_t = \frac{\rho k}{\mu \omega} \quad (17)$$

and

$$\sigma_k = 2 \quad \alpha_0^* = \beta/3 \quad R_s = 8 \quad R_\omega = 2.7$$

$$\sigma_\omega = 2 \quad \alpha_0 = 1/10 \quad R_k = 6$$

The compressibility correction is given by

$$F(M_t) = \text{Maximum}(M_t^2 - M_{t0}^2, 0.0)$$

where the turbulent Mach number is the same as before, and the constants default to  $\xi_k = 1.0$ ,  $\xi_\omega = 0.0$ , and  $M_{t0} = 0.00$ .

By comparing the k- $\omega$  and the k- $\epsilon$  models, a relation between  $\omega$  and  $\epsilon$  can be found. Wilcox<sup>5</sup> defines this relation as  $\omega = \epsilon/(\beta^* k)$ . In the results to be presented

below, comparisons are made between the models using this relation. However, since  $\beta^*$  is a function of  $Re_t$ , which in turn depends upon  $\omega$ , the conversion of  $\epsilon$  to  $\omega$  makes the assumption that  $\beta^* = 0.09$ .

### Code Modifications and Usage

Because of the similarity in the k- $\epsilon$  and k- $\omega$  formulations, the current implementation makes use of the existing Chien k- $\epsilon$  algorithm available in NPARC. The algorithm for solving the k- $\epsilon$  equations dates back to the work of Nichols<sup>19</sup> with recent modifications by Georgiadis, Chitsomboon, and Zhu.<sup>20</sup> The most significant changes occurred in the calculation of the source terms involved in the k- and  $\omega$ -equations. The source terms are those on the right-hand side of equations (10) and (11) excluding the diffusion terms.

The k- $\omega$  model is selected by setting IMUTUR (or IMUTR2) equal to 7. Since it is similar in form to the k- $\epsilon$  model and uses the same solution algorithm, users should expect stability and convergence to be comparable. Users are advised to use appropriate near-wall grid spacing along viscous surfaces. This helps to resolve the boundary layer and the large  $\omega$ -gradients which occur near these surfaces.

### Compressibility Corrections

A compressibility correction has been added to the model equations to enhance predictions at higher Mach numbers. The corrections described by Sarkar<sup>17</sup> or Wilcox<sup>21</sup> may be selected by setting the variables COMPK, COMPW, and CMT0 according to the following table:

COMPK	COMPW	CMT0	Correction type
1.0	0.0	0.00	Sarkar (k-eq.) <sup>a</sup>
1.0	1.0	0.00	Sarkar (k+ $\omega$ eqs.)
1.5	1.5	0.25	Wilcox
0.0	0.0	0.00	None

<sup>a</sup>Default.

These variables correspond to  $\xi_k$ ,  $\xi_\omega$ , and  $M_{t0}$ , respectively, in equations (10) and (11) and have been included in the TURBIN namelist block. As discussed in reference 21, the Sarkar correction only affects the k-equation in the k- $\epsilon$  model. When used with the k- $\omega$  model, however, corrections should be added to both the k- and  $\omega$ -equations. Computations for the Sajben<sup>22</sup> diffuser strong-shock case

(discussed in the Results section) indicate that adding the Sarkar correction to only the k-equation provides the best results. The Wilcox correction was of little use since the turbulent kinetic energy led to an  $M_t$  value that was below the cutoff turbulent Mach number  $CMT0 = 0.25$ . As a result, the Sarkar correction to the k-equation was chosen as the default setting, but the other options have been included because of the lack of extensive testing of high-speed flows. These options should provide the greatest amount of flexibility and limit future code modifications.

### Boundary Conditions

The boundary value for  $\omega$  along a viscous wall is related to the surface roughness of the wall. This relation is given by Wilcox:<sup>5</sup>

$$\omega = \frac{u_\tau^2}{\nu} S_R \quad \text{at } y = 0 \quad (18)$$

where

$$S_R = \begin{cases} \left( \frac{50}{k_R^+} \right)^2, & k_R^+ < 25 \\ \frac{100}{k_R^+}, & k_R^+ \geq 25 \end{cases} \quad (19)$$

and is valid for  $k_R^+ = u_\tau k_R / \nu$  values up to 400. The NPARC code has been modified to allow the user to input the wall surface roughness for no-slip walls. This value is read in through the auxiliary pressure variable. The variable SRDEF has been added to the TURBIN namelist block and is used to specify the default smooth-wall surface roughness. When this variable is used, the surface roughness along all the viscous boundaries can be adjusted at once. The hydraulically smooth  $k_R^+$  value of 1.0 is the default value. In specifying the surface roughness for either input, values greater than zero are treated as  $k_R^+$  and values less than zero are treated as  $k_R$  (average sand-grain surface roughness nondimensionalized by the reference length). According to reference 23, the effective sand-grain surface roughness is classified as follows:

$k_R^+ \leq 5$	Hydraulically smooth
$5 \leq k_R^+ \leq 70$	
$70 \leq k_R^+ \leq 400$	Transitional

The NPARC code computes the  $k_R^+$  value specified for the individual boundary through the auxiliary pressure variable and compares it with the smooth-wall value given by SRDEF. It then uses the larger of these values to compute  $\omega$  at the boundary. Failure to specify the auxiliary pressure will result in a  $k_R$  value of zero (default), and computations will be performed using the default surface roughness given by SRDEF. Because boundary conditions 62 and 68 use the auxiliary pressure variable for other purposes, the surface roughness given by SRDEF is used. No calculations have been performed using any surface roughness value other than the default value ( $k_R^+ = 1.0$ ), and *users are advised* to do the same until such time as this option can be more fully investigated.

All other boundary conditions remain unchanged. As with the k- $\epsilon$  model, the turbulent quantities are extrapolated from the interior of the flow field along slip walls and at free boundaries. Values of turbulence intensity  $I$  and turbulent viscosity  $\mu_t$  may be specified for free inflow boundaries as described by Georgiadis, Chitsomboon, and Zhu.<sup>20</sup> Using a fixed inflow will cause the turbulent quantities along that boundary to remain unchanged from those in the restart file.

### Stability Considerations

The limiters used by NPARC to increase convergence and stability by capping the values of the turbulent quantities at both the high and low extremes were modified to accommodate the k- $\omega$  model. These limiters are used on the interior of the flow field, not along boundaries. The current implementation is similar to that used by the k- $\epsilon$  model, but because  $\omega$  approaches infinity near a smooth viscous boundary, numerical stability problems may arise if it is limited in this region. In regions where the turbulent kinetic energy is found to be very small,  $k$  is set to a minimum value, but  $\omega$  is not changed. If  $\omega$  becomes too small, both  $k$  and  $\omega$  are set to minimum values. Should the turbulent kinetic energy exceed the maximum value given by  $k_{\max} = 0.10 \times U_{\text{ref}}^2 (k-\epsilon)$ , it is set to the maximum value and  $\omega$  is computed using

$$\omega = \text{Maximum}(\omega - \text{Calculated}; \alpha^* \rho k_{\max} / \mu_{t,\max})$$

where  $\mu_{t,\max}$  is specified through the user input TMUMAX. No upper limit check is made on  $\omega$ . Users who experience convergence difficulties or erroneous results should check to make sure the upper limits for the turbulent kinetic energy (adjusted through the variable UREFKE) and the turbulent viscosity (adjusted through TMUMAX) are set sufficiently high. The output file (26) lists the iteration number and the number of points where the turbulent quantities are limited by  $k_{\min}$ ,  $k_{\max}$ , and  $\omega_{\min}$ .

We found that near regions of rapid acceleration or deceleration, such as near leading edges and behind shock waves, the turbulent viscosity can become very large. The variable  $C_\mu$  option in the  $k$ - $\epsilon$  model has been modified for use in the  $k$ - $\omega$  model and has helped to alleviate this problem. The modification involves scaling the turbulent viscosity based on the ratio of production to dissipation  $R$  as:

$$\mu_t = \frac{0.10738}{0.09} \frac{(0.64286 + 0.19607R)}{[1 + 0.357(R - 1)]^2} \alpha^* \frac{\rho k}{\omega} \quad (20)$$

Details of the formulation may be found in reference 24. Even though the variable  $C_\mu$  option may be turned on or off in the  $k$ - $\epsilon$  model by adjusting the value of ICMU, it has been included in the  $k$ - $\omega$  model regardless. Results for the cases discussed next were not adversely affected by this modification. In fact, some results showed a slight improvement.

#### Example 1

Consider the two-dimensional flow over a smooth flat plate. For a  $111 \times 81$  grid the NPARC2D formatted input file is given as

```
&TURBIN
IMUTUR=2,    IFMAX=1,
NTURB=5200,  IMUTR2=7,
&END
&BLOCK
INVISC(1)=1, LAMIN(1)=0, NBCSEG=5,
INVISC(2)=1, LAMIN(2)=1,
&END
```

```
1 15 1 1 50 1
16 111 1 1 60 1
1 111 81 81 50 -1
111 111 2 80 0 -1 0.7143 1.0000
1 1 2 80 0 1 0.7345 1.0080
```

In this example, the  $k$ - $\omega$  model will be initialized from the Baldwin-Lomax model at iteration 5200 (assuming the current iteration NC is less than 5200). The first 15 grid points are treated as a slip wall to allow for a uniform profile at the leading edge of the flat plate. The inflow and outflow boundaries are both free boundaries. The free stream is modeled using a slip boundary that is far from the flat plate so as not to disturb the boundary layer. The flat plate is smooth, and the default surface roughness is used. Since no compressibility corrections have been specified, the default setting (Sarkar's correction to the  $k$ -equation) will be used.

#### Example 2

Next, consider a two-dimensional channel flow to be computed on a  $101 \times 51$  grid. The formatted inputs for this flow are given as

```
&INPUTS
NC=5000,
&END
&TURBIN
IMUTUR=4,    IMUTR2=7,    NTURB=5200,
COMPKE=1.5,  COMPW=1.5,    CMT0=0.25,
SRDEF=1.0,
&END
&BLOCK
INVISC(1)=1, LAMIN(1)=0,    NBCSEG=5,
INVISC(2)=1, LAMIN(2)=1,
&END
```

```
1 1 2 50 0 1 0.7000 1.0000
101 101 2 50 0 -1 0.6000 0.9800
1 31 1 1 60 1
32 101 1 1 60 1 50.0000
1 101 51 51 61 -1 -0.0001 0.9900
```

In this case, the  $k$ - $\omega$  model will be initialized from the  $k$ - $\epsilon$  solution at iteration 5200. To do so, IMUTUR is set to the  $k$ - $\epsilon$  model and the current iteration is reset to a value lower than NTURB (on subsequent runs, NC should be set to -1). If NC is not set below NTURB for the initial run, NPARC will read in  $k$ ,  $\epsilon$ , and  $\mu_t$  believing them to be  $k$ ,  $\omega$ , and  $\mu_t$ . However, the values of  $\epsilon$  and  $\omega$  can differ by several orders of magnitude, and this may result in poor convergence or erroneous results or both. The compressibility correction of Wilcox has been chosen to override the Sarkar default settings. The minimum allowable surface roughness SRDEF has been set to a  $k_R^+$  value of 1 (which is what the default value would have been had this line been omitted). The lower boundary has been specified as a no-slip adiabatic surface. Since no surface roughness has been specified for the first 31 grid points, the default roughness given by SRDEF will be used. Along the remainder of the lower wall, a  $k_R^+$  value of 50.0 will be used. The upper boundary is a no-slip isothermal wall. Along this boundary, a surface roughness  $k_R$  (nondimensionalized by the reference length) of 0.0001 will be used. If the  $k_R^+$  value corresponding to this  $k_R$  at any point along this boundary becomes less than the smooth-wall surface roughness given by SRDEF ( $k_R^+ = 1.0$ ), the value of SRDEF will be used instead.

## Results

### Smooth Flat Plate

Incompressible flow over a smooth flat plate was used as an initial test case for the  $k-\omega$  model. A  $111 \times 81$  grid was used to model a Mach 0.2 flow. The first 15 grid points were treated as a slip wall in order for the flow to reach the leading edge of the flat plate with a uniform profile. The grid was sufficiently packed in the streamwise direction to resolve the flow gradients at the leading edge of the flat plate and normal to the surface to resolve the boundary layer. The  $k-\omega$  solution was initiated from the Baldwin-Lomax algebraic model by assuming that the production in turbulent kinetic energy was equal to the dissipation rate. The solution was determined to be converged when fluctuations in the mean flow and turbulent quantities at the last streamwise coordinate ceased. This corresponded to a drop in the L2 residual error of four orders of magnitude.

Figure 1 shows the variation in skin friction coefficient  $C_f$  along the flat plate. Both the  $k-\epsilon$  and  $k-\omega$  models give similar results and overpredict the skin friction as compared with the experimental data of Wieghardt.<sup>25</sup> Figures 2 to 5 show the turbulent quantities and velocities at  $Re_x$  values of  $1 \times 10^6$ ,  $4 \times 10^6$ , and  $1 \times 10^7$ . From the turbulent kinetic energy profiles presented in figure 2, the maximum value predicted by the  $k-\omega$  model is less than that of the  $k-\epsilon$  model. This was also true in the investigation conducted by Lang and Shih.<sup>18</sup> Figure 3 indicates close agreement in the turbulent viscosity values predicted by each model close to the wall. The large differences between the maximum values do not have a dramatic effect on the turbulent shear stress, as shown in figure 4. The small discontinuity in the Baldwin-Lomax results is caused by the turbulent viscosity, which is not smooth at the location where the inner and outer layers of the model meet. The velocity profiles presented in figure 5 compare well with the  $k-\epsilon$  model and the experimental data of references 26 and 27. Results from the three-dimensional code (fig. 6) were nearly identical to the two-dimensional results, except for a small deviation near the leading edge of the flat plate.

At no time while running this test case was  $\omega$  observed to be limited near the viscous wall. Both  $k$  and  $\omega$  reached minimum allowable values in the free stream, as should be expected. The large difference in  $\omega$ -values of the slip wall and flat plate solutions did not present any numerical stability difficulties.

### Fraser Diffuser

Having found that the  $k-\omega$  model works as well as the  $k-\epsilon$  model for the flat plate, the model was then examined for an adverse pressure gradient test case. The conical

diffuser of Fraser<sup>28</sup> represents one of the simplest of these types of flows. This flow enters a reducing section after which it passes through a straight pipe (fig. 7(a)). Here the subsonic flow is tripped so that it becomes fully turbulent before entering the  $5^\circ$  half-angle diverging channel. Experimental results indicate that the flow very nearly reaches separation at the diffuser exit.

A computational grid with 121 axial and 71 radial points was used to model this axisymmetric flow (fig. 7(b)). A small circular arc was used as a transition between sections to promote grid orthogonality. The grid was also clustered near the walls and the inflow to resolve gradients in these regions. The inflow was modeled using a free boundary, and the outflow was specified through the use of the mass-flux boundary condition. Both the  $k-\epsilon$  and  $k-\omega$  models were initialized from a Baldwin-Lomax solution. The three-dimensional  $k-\omega$  results were initialized by mapping the Baldwin-Lomax axisymmetric solution onto a three-dimensional grid. Fifteen planes were used in the circumferential direction to model one quarter of the flow. This test was performed to validate the ability of the three-dimensional code to model an axisymmetric flow.

Figure 8 compares the velocity profiles of each of the models at two axial locations. The skin friction along the diffuser wall is given in figure 9. Both the Baldwin-Lomax and Baldwin-Barth models predict a separation beginning roughly halfway through the diffuser. The  $k-\epsilon$  model shows little sensitivity to the adverse pressure gradient and predicts a very well attached flow. The  $k-\omega$  model, however, is much more accurate at predicting the near separation at the diffuser exit. Results from the three-dimensional NPARC code were found to be nearly identical to the two-dimensional results.

### Sajben Diffuser

The Sajben<sup>22</sup> diffuser weak- and strong-shock cases were selected as the next validation cases for several reasons: (1) They furnish an additional test for the  $k-\omega$  model in an adverse pressure gradient. (2) They are compressible flow cases and provide an opportunity to investigate the compressibility corrections of Sarkar and Wilcox. (3) They involve a shock-induced separation and are more indicative of the types of flows many NPARC users investigate.

The Sajben geometry is shown in figure 10(a), and the  $81 \times 51$  grid on which both cases were computed is shown in figure 10(b). Both the inflow and outflow boundaries were specified as free boundaries. Computations on the weak-shock case were performed first with the  $k-\epsilon$  and  $k-\omega$  models initialized from the Baldwin-Lomax solution. The outflow pressure of the  $k-\epsilon$  and  $k-\omega$  solutions was then lowered to obtain the corresponding strong-shock results. The three-dimensional solutions were initialized by

copying the corresponding two-dimensional solution onto consecutive planes. Comparisons of the three-dimensional and two dimensional results are made using the middle plane.

**Weak Shock.**—Figure 11 shows the pressure distributions along the top and bottom surfaces of the diffuser. The results from the various models are basically the same with the exception of the shock location. The  $k-\epsilon$  model predicts the earliest shock, followed by the Baldwin-Lomax and  $k-\omega$  models. Both the  $k-\epsilon$  and Baldwin-Lomax models compare well with the experimental data, while the  $k-\omega$  model predicts the shock location slightly further downstream.

Figure 12 displays the velocity profiles at two locations downstream of the shock. From these profiles, it can be seen that the  $k-\epsilon$  model predicts a larger core velocity, while the  $k-\omega$  model is more accurate in the near-wall regions. A comparison of the results obtained using the two- and three-dimensional versions of NPARC is given in figure 13. Both give similar results.

**Strong Shock.**—The top and bottom wall pressure distributions for the strong-shock case are given in figure 14. These results show that downstream of the shock, the Baldwin-Lomax model has difficulties converging to a steady-state solution for this case, and the results presented represent an instant in time. Examining the two-equation models reveals that the  $k-\omega$  model still predicts the shock location further downstream than the data suggest, but it does a much better job predicting the pressure distribution in the separation region.

Velocity profiles downstream of the shock location are given in figures 15(a) to (c). Although none of the models accurately predicts the velocity profile near the upper wall, the  $k-\omega$  model provides the best agreement. It also gives very good results along the lower boundary. Both the  $k-\epsilon$  and  $k-\omega$  models predict roughly the same peak velocity, but the  $k-\omega$  model more accurately matches the core-flow profile. Results from the two- and three-dimensional codes were again found to be nearly identical (fig. 16).

A comparison made of the different compressibility corrections to the  $k-\omega$  model is given in figure 17. Adding the Sarkar correction to only the  $k$ -equation gives the best results. This setting was selected as the default setting. Using the correction of Wilcox yields nearly the same results as not using any compressibility correction. This occurs because the turbulent kinetic energy is such that the turbulent Mach number at all but a very few points is below the cut off Mach number given by CMT0.

## Conclusions and Future Work

The  $k-\omega$  model was recently implemented in the NPARC code. Results from the validation cases indicate that this model is better suited to adverse pressure gradient flow calculations than are other turbulence models currently available in NPARC. A description of the model equations and boundary conditions was given along with a discussion of several other model features not completely validated in this study. Future work using this model will include further validation and an examination of the model's ability to simulate transition and surface roughness.

## References

1. Jones, W.P.; and Launder, B.E.: The Prediction of Laminarization With a Two-Equation Model of Turbulence. *Int. J. Heat Mass Transfer*, vol. 15, 1972, pp. 301–314.
2. Launder, B.E.; and Spalding, D.B.: The Numerical Computation of Turbulent Flows. *Comp. Methods Appl. Mech. Eng.*, vol. 3, 1974, pp. 269–289.
3. Kolmogorov, A.N.: Equations of Turbulent Motion of an Incompressible Fluid. *Izv. Ak. Nauk. SSSR. Ser. fizicheskaya*, vol. 4, no. 1–2, 1942, pp. 56–58.
4. Menter, F.R.: Improved Two-Equation  $k-\omega$  Turbulence Models for Aerodynamic Flows. NASA TM-103975, 1992.
5. Wilcox, D.C.: Simulation of Transition With a Two-Equation Turbulence Model. *AIAA J.*, vol. 32, no. 2, Feb. 1994, pp. 247–255.
6. Wilcox, D.C.: A Half Century Historical Review of the  $k-\omega$  Model. AIAA Paper 91-0615, Jan. 1991.
7. Wilcox, D.C.: Reassessment of the Scale-Determining Equation for Advanced Turbulence Models. *AIAA J.*, vol. 26, no. 11, Nov. 1988, pp. 1299–1310.
8. Wilcox, D.C.: Comparison of Two-Equation Turbulence Models for Boundary Layers With Pressure Gradient. *AIAA J.*, vol. 31, no. 8, Aug. 1993, pp. 1414–1421.
9. Cooper, G.K.; and Sirbaugh, J.R.: The PARC Distinction: A Practical Flow Simulator. AIAA Paper 90-2002, July 1990.
10. Beam, R.M.; and Warming, R.F.: An Implicit Finite-Difference Algorithm for Hyperbolic Systems in Conservation-Law Form. *J. Comp. Phys.*, vol. 22, no. 1, 1976, pp. 87–110.

11. Cooper, K.: NPARC 2.0—Features and Capabilities, AIAA Paper 95-2609, July 1995.
12. Thomas, P.D.: Numerical Method for Predicting Flow Characteristics and Performance of Nonaxisymmetric Nozzles, Theory. NASA CR-3147, Sept. 1979.
13. Baldwin, B.; and Lomax, H.: Thin-Layer Approximation and Algebraic Model for Separated Turbulent Flows. AIAA Paper 78-257, Jan. 1978.
14. Martinelli, L.; and Yakhot, V.: RNG-Based Turbulence Transport Approximations With Applications to Transonic Flows Renormalization Group Theory. AIAA Paper 89-1950, 1989.
15. Baldwin, B.S.; and Barth, T.J.: A One-Equation Turbulence Transport Model for High Reynolds Number Wall-Bounded Flows. NASA TM-102847, 1990.
16. Chien, K.-Y.: Predictions of Channel and Boundary-Layer Flows With a Low-Reynolds-Number Turbulence Model. AIAA J., vol. 20, no. 1, Jan. 1982, pp. 33-38.
17. Sarkar, S.; and Balakrishnan, L.: Application of a Reynolds Stress Turbulence Model to the Compressible Shear Layer. AIAA Paper 90-1465, 1990.
18. Lang, N.J.; and Shih, T.H.: A Critical Comparison of Two-Equation Turbulence Models. NASA TM-105237, 1991.
19. Nichols, R.H.: A Two-Equation Model for Compressible Flows. AIAA Paper 90-0494, Jan. 1990.
20. Georgiadis, N.J.; Chitsomboon, T., and Zhu, J.: Modification of the Two-Equation Turbulence Model in NPARC to a Chien Low Reynolds Number  $k$ - $\epsilon$  Formulation. NASA TM-106710, 1994.
21. Wilcox, D.C.: Dilatation-Dissipation Corrections for Advanced Turbulence Models. AIAA J., vol. 30, no. 11, Nov. 1992, pp. 2639-2646.
22. Sajben, M.; and Kroutil, J.C.: Effects of Initial Boundary-Layer Thickness on Transonic Diffuser Flows. AIAA J., vol. 19, no. 11, 1981, pp. 1386-1393.
23. Cebeci, T.; and Bradshaw, P.: Physical and Computational Aspects of Convective Heat Transfer, Springer-Verlag, New York, 1984.
24. Rodi, W.: A New Algebraic Relation for Calculating the Reynolds Stresses. Z. Ang. Math. Mech. vol. 56, 1976, pp. T219-T221.
25. Wiegardt, K.; and Tillmann, W.: On the Turbulent Friction Layer for Rising Pressure. NACA TM-1314, 1952.
26. Reichardt, H.: Heat Transfer Through Turbulent Friction Layers. NACA TM-1047, 1943.
27. Klebanoff, P.S.; and Diehl, Z.W.: Some Features of Artificially Thickened Fully Developed Turbulent Boundary Layers With Zero Pressure Gradient. NACA TN-2475, Oct. 1951.
28. Fraser, H.R.: The Turbulent Boundary Layer in a Conical Diffuser, J. Hydraulics Div., Proceedings of the American Society of Civil Engineers, June 1958, pp. 1684/1-1684/17.

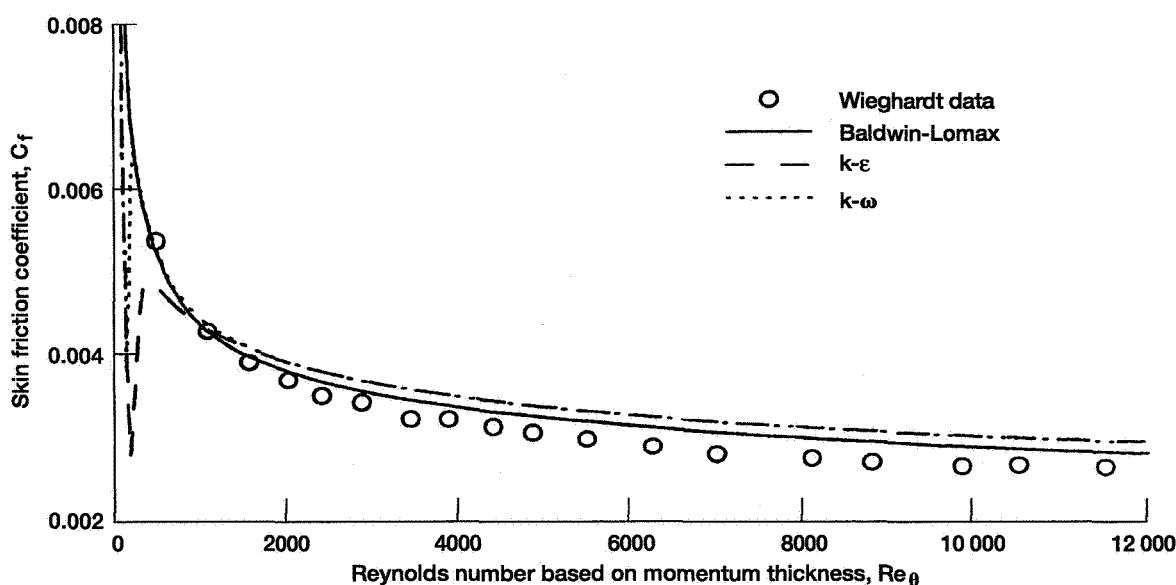


Figure 1.—Local skin friction coefficient along flat plate.

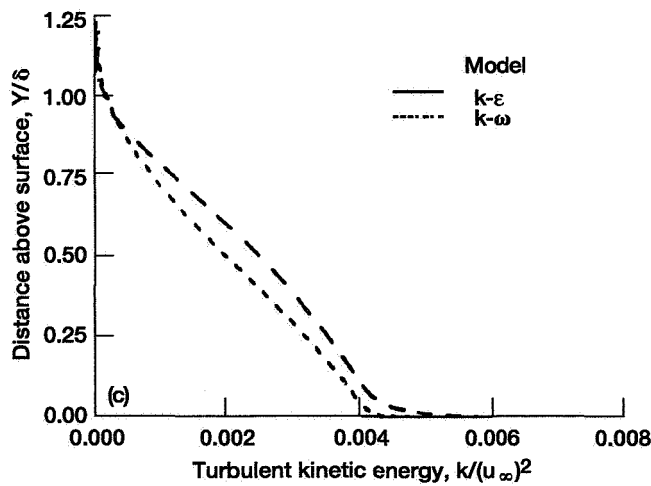
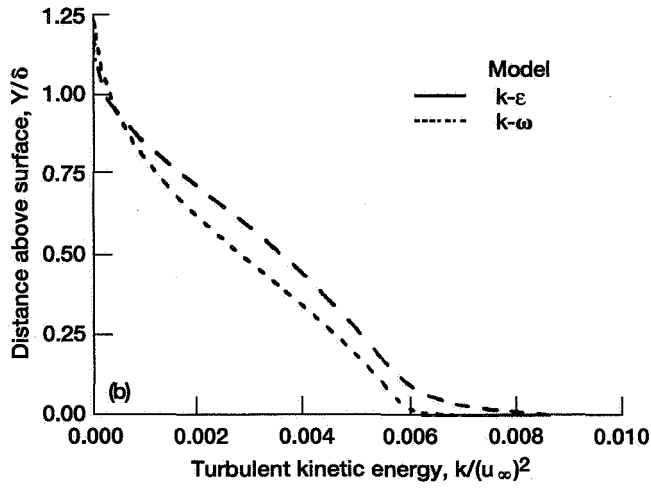
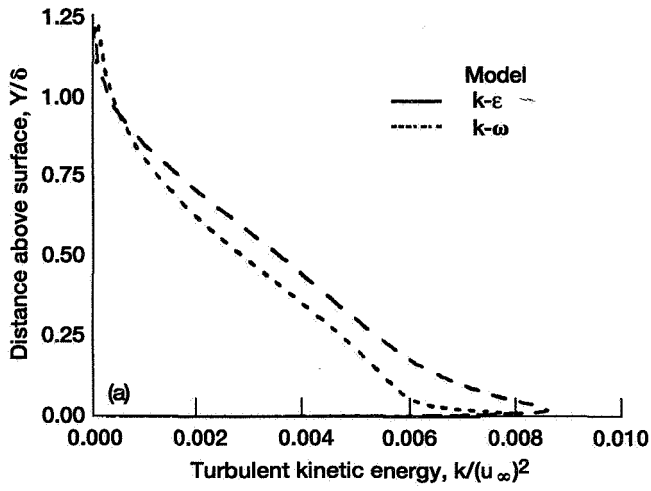


Figure 2.—Turbulent kinetic energy profiles along flat plate for Reynolds number based on plate location  $Re_x$ .  
(a)  $Re_x = 1 \times 10^6$ . (b)  $Re_x = 4 \times 10^6$ . (c)  $Re_x = 1 \times 10^7$ .

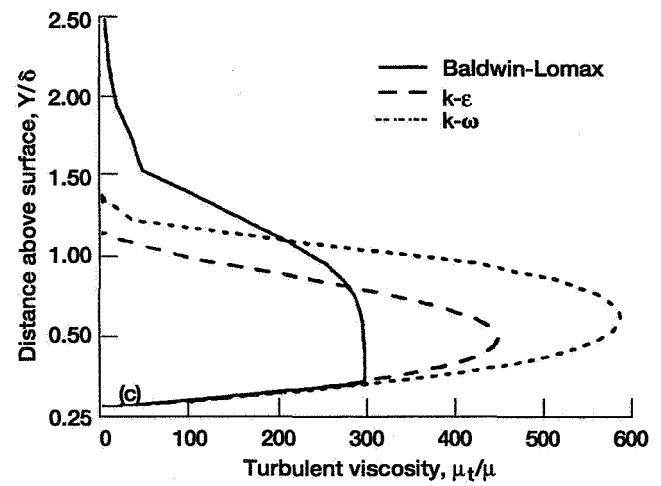
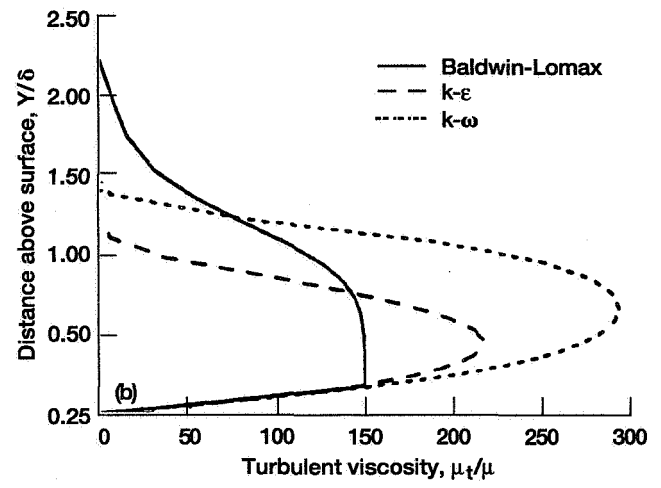
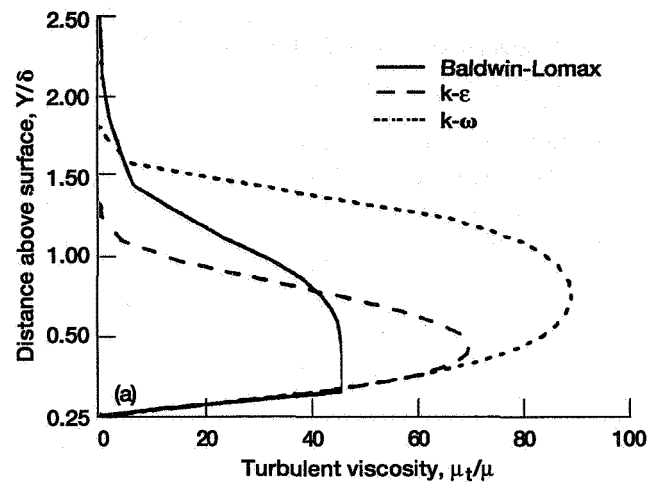


Figure 3.—Turbulent viscosity profiles along flat plate for Reynolds number based on plate location  $Re_x$ .  
(a)  $Re_x = 1 \times 10^6$ . (b)  $Re_x = 4 \times 10^6$ . (c)  $Re_x = 1 \times 10^7$ .

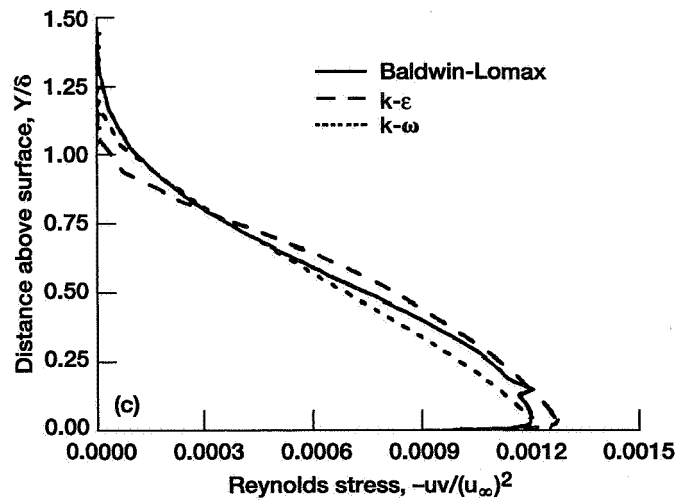
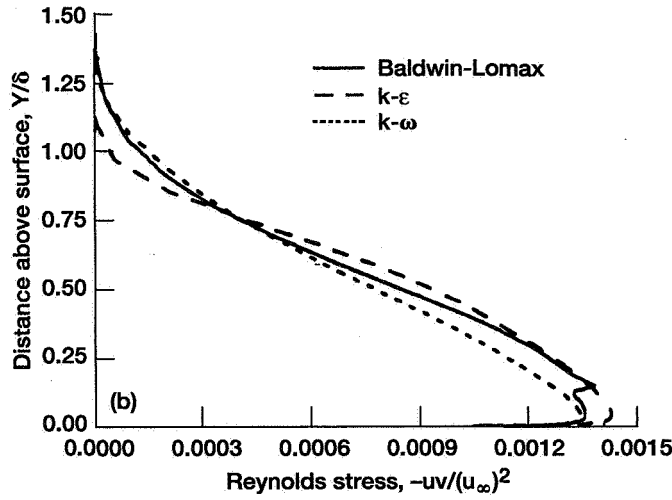
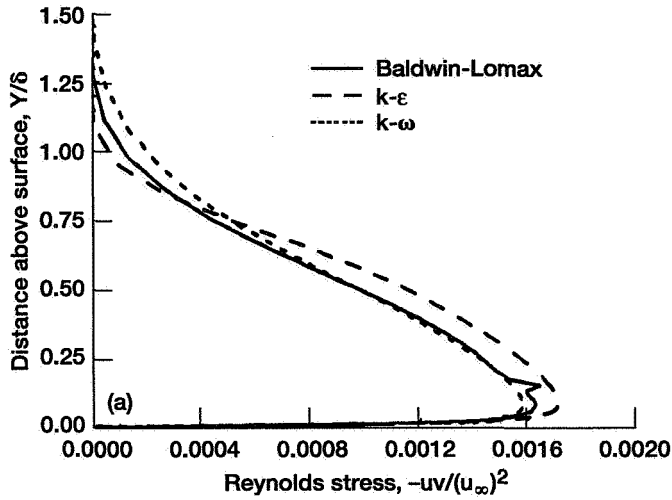


Figure 4.—Turbulent shear stress along flat plate for Reynolds number based on plate location  $Re_x$ . (a)  $Re_x = 1 \times 10^6$ . (b)  $Re_x = 4 \times 10^6$ . (c)  $Re_x = 1 \times 10^7$ .

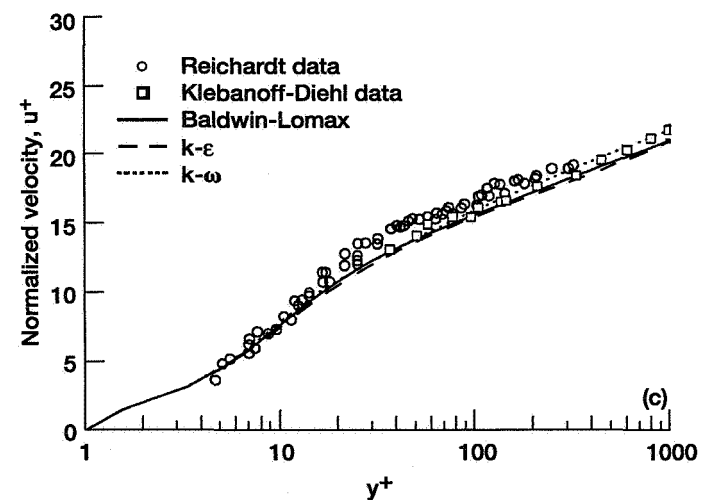
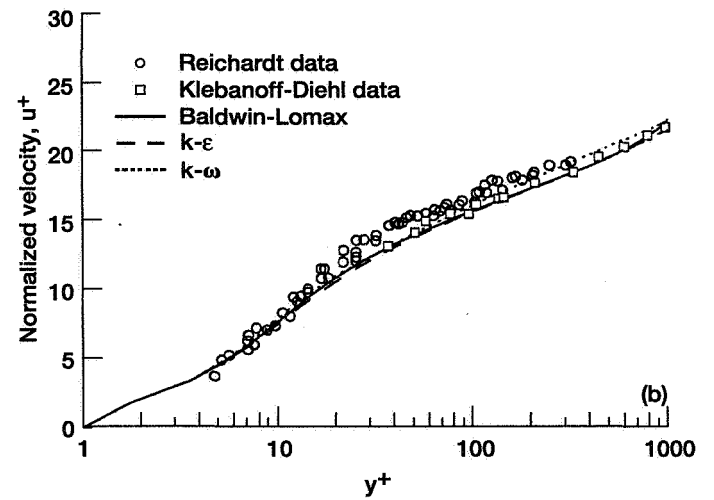
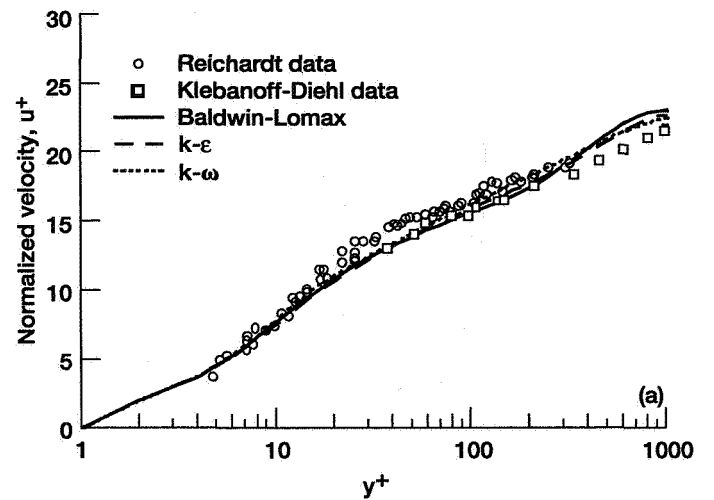


Figure 5.—Velocity profiles along flat plate for Reynolds number based on plate location  $Re_x$ . (a)  $Re_x = 1 \times 10^6$ . (b)  $Re_x = 4 \times 10^6$ . (c)  $Re_x = 1 \times 10^7$ .

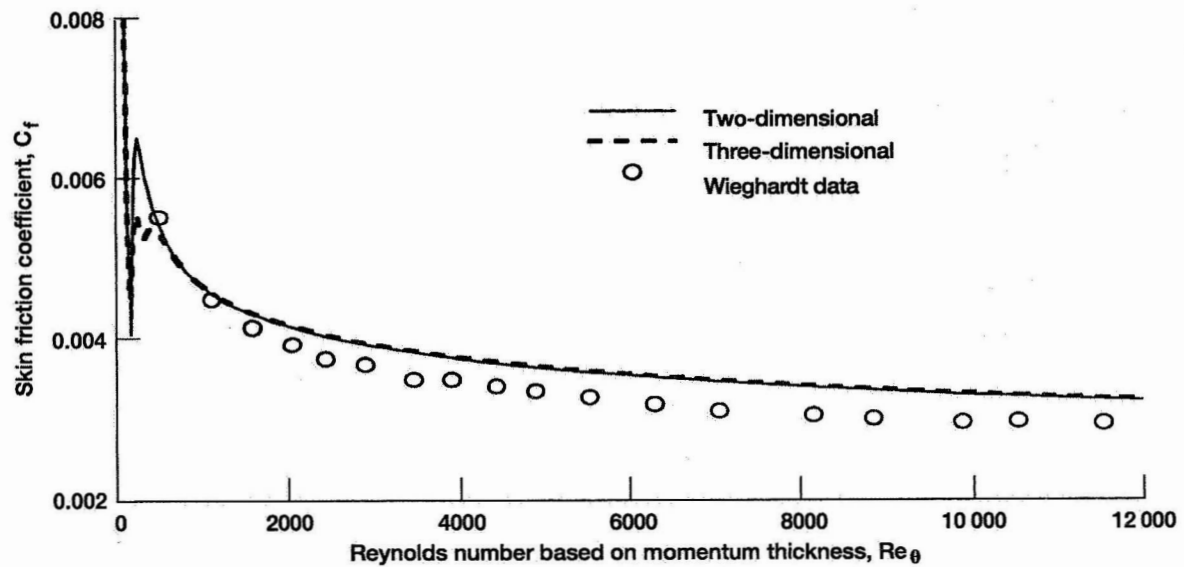


Figure 6.—Comparison of two- and three-dimensional  $k-\omega$  skin friction results for flat plate.

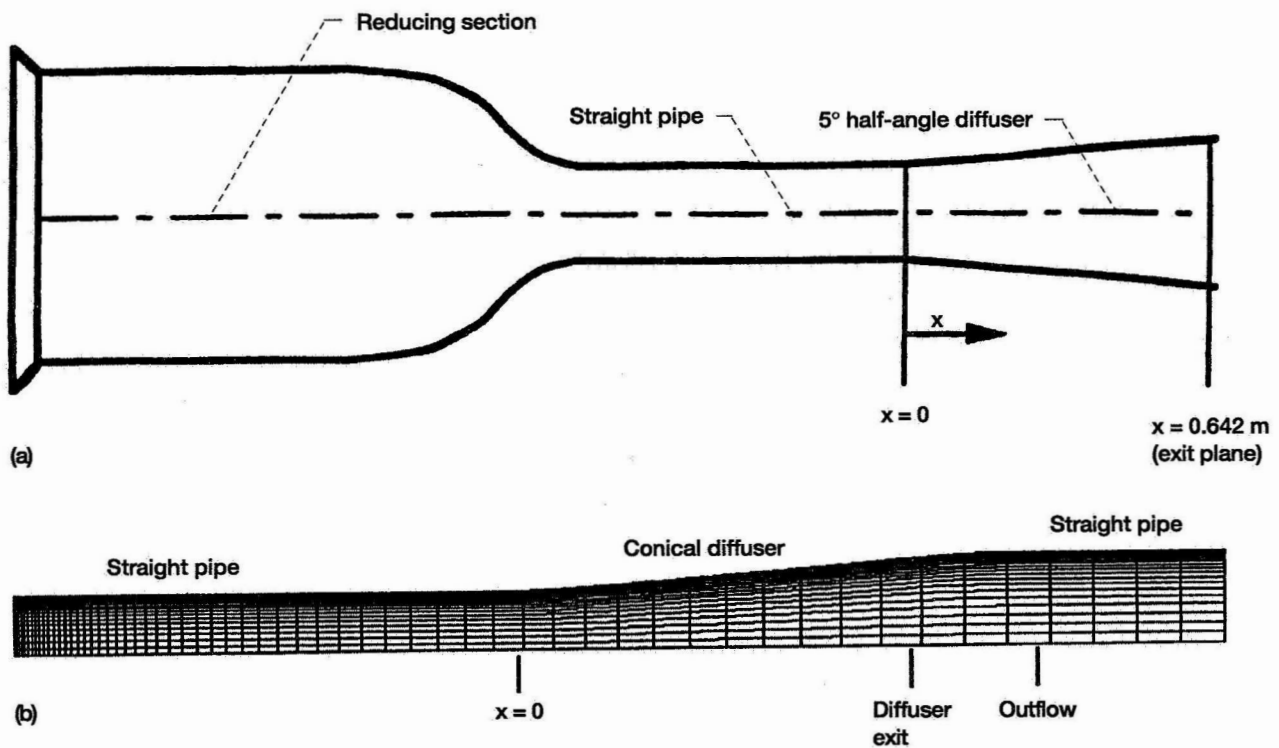


Figure 7.—Fraser diffuser. (a) Geometry. (b) Computational mesh.

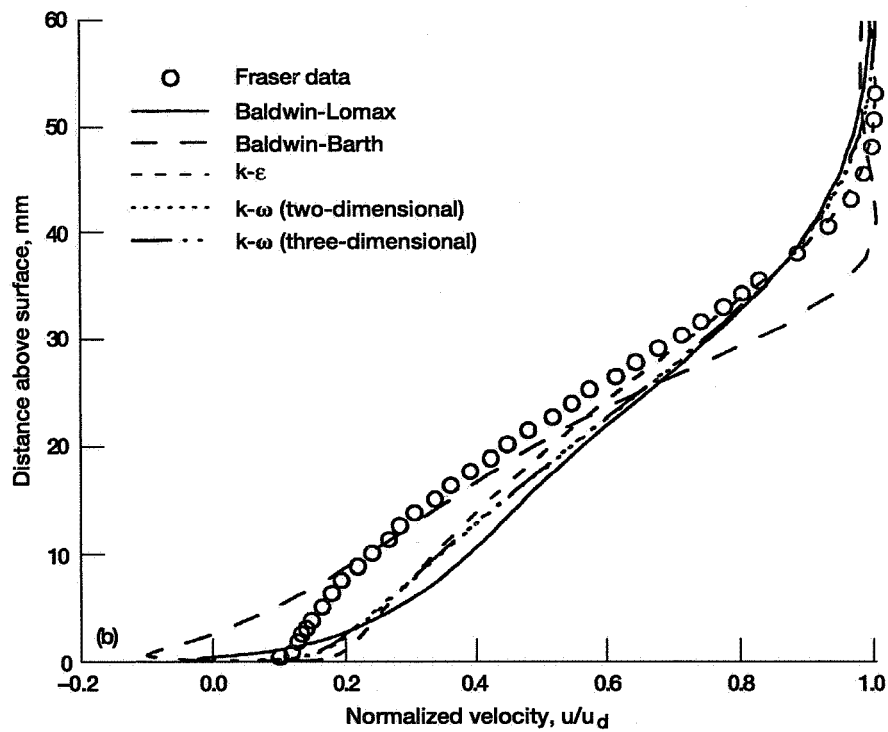
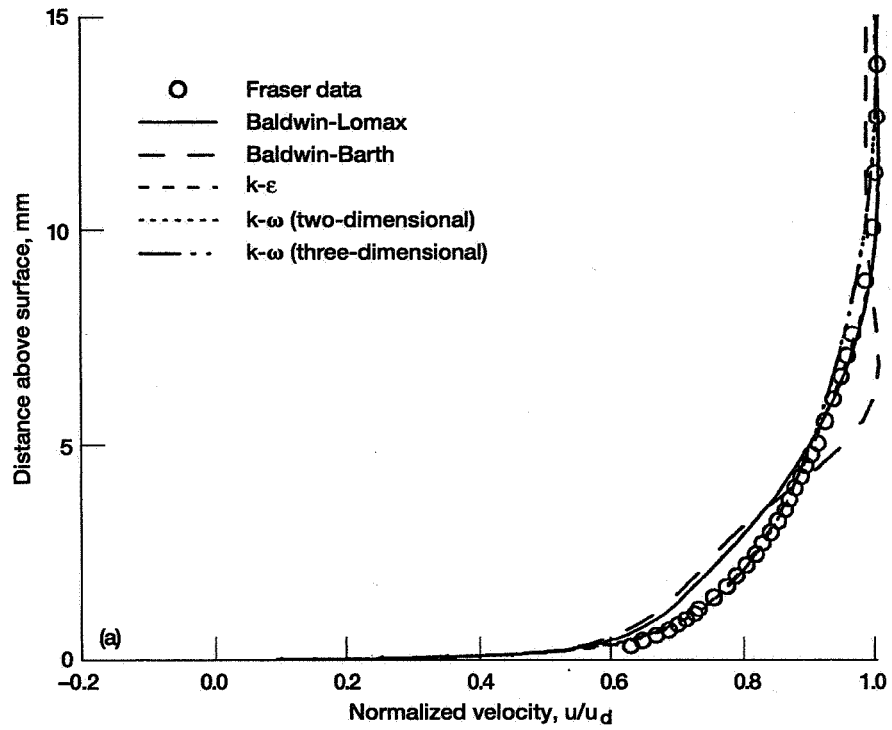


Figure 8.—Fraser diffuser profiles at two axial locations  $x$ . (a)  $x = 117$  mm.  
(b)  $x = 642$  mm.

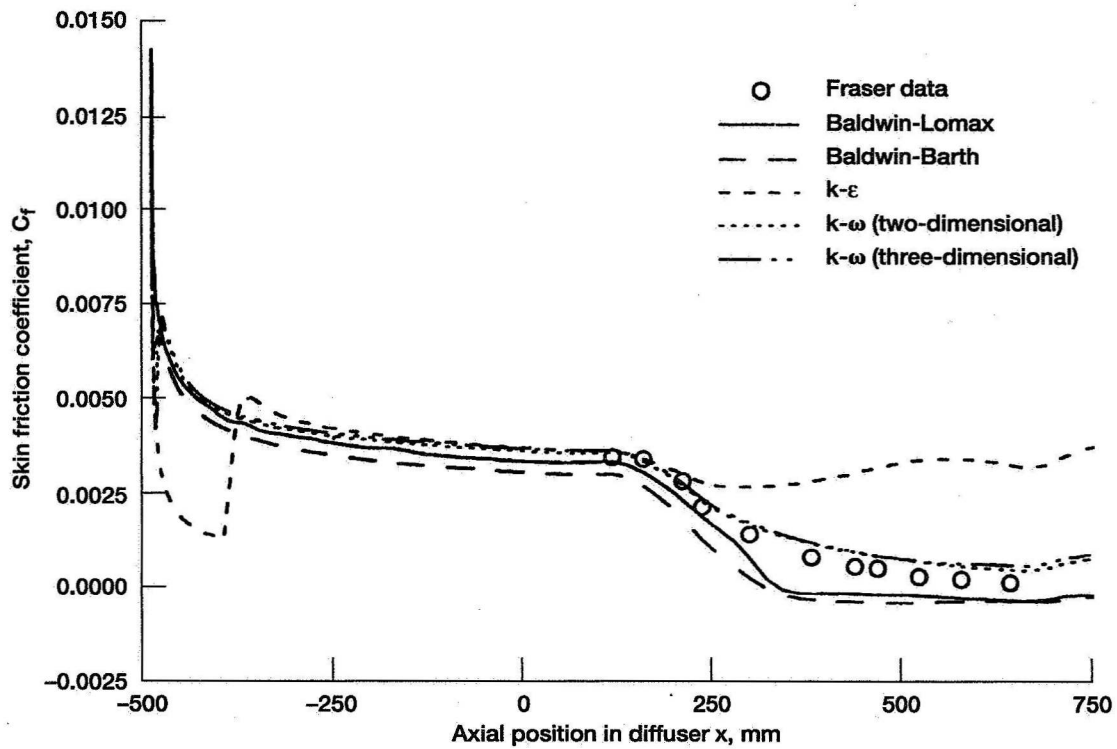


Figure 9.—Skin friction for Fraser diffuser.

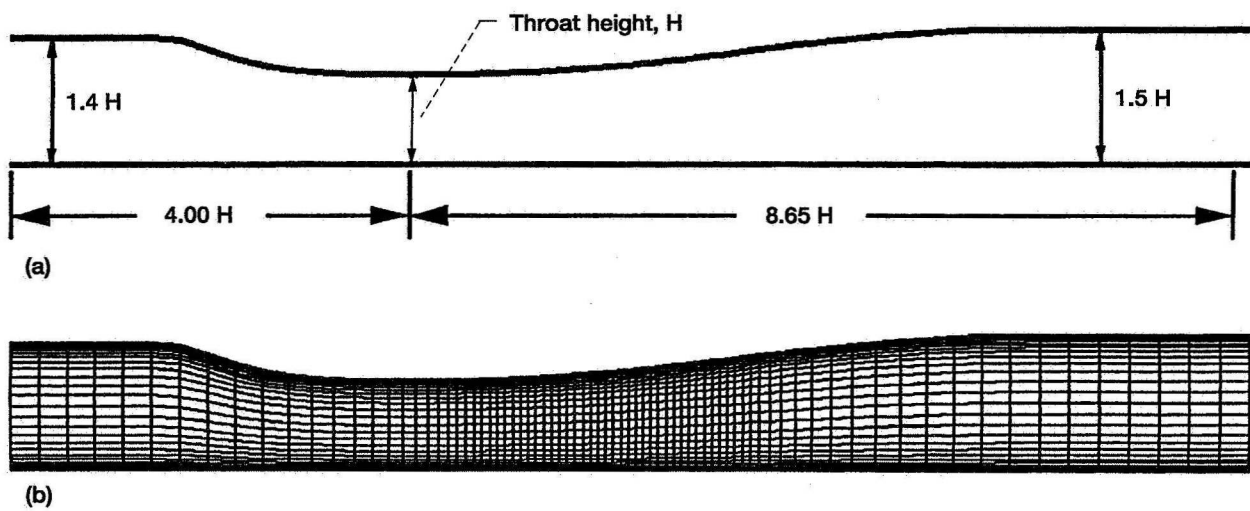


Figure 10.—Sajben diffuser. (a) Geometry. (b) Computational mesh.

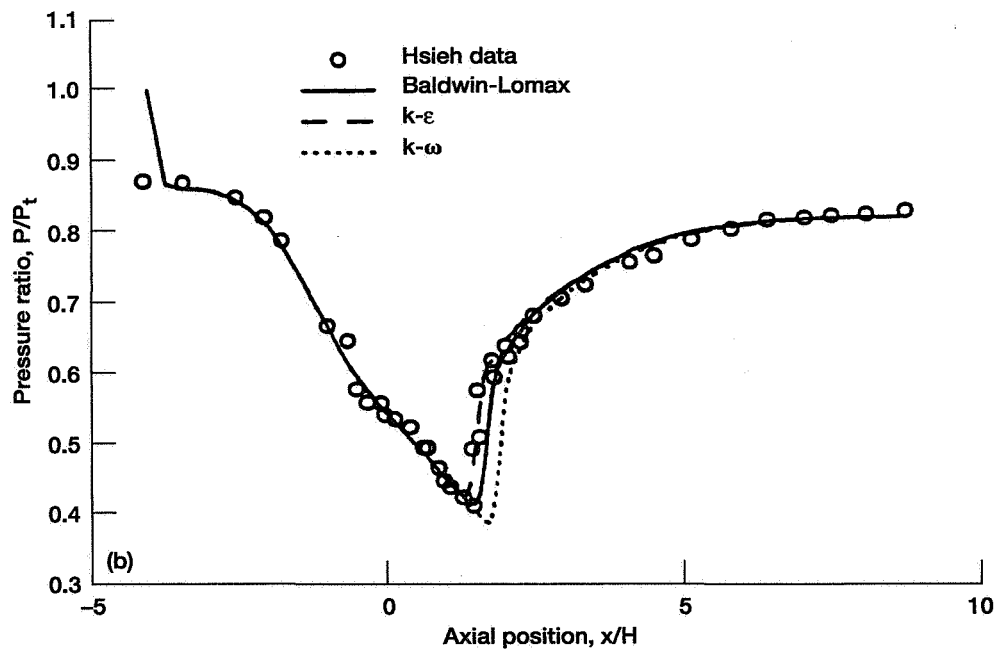
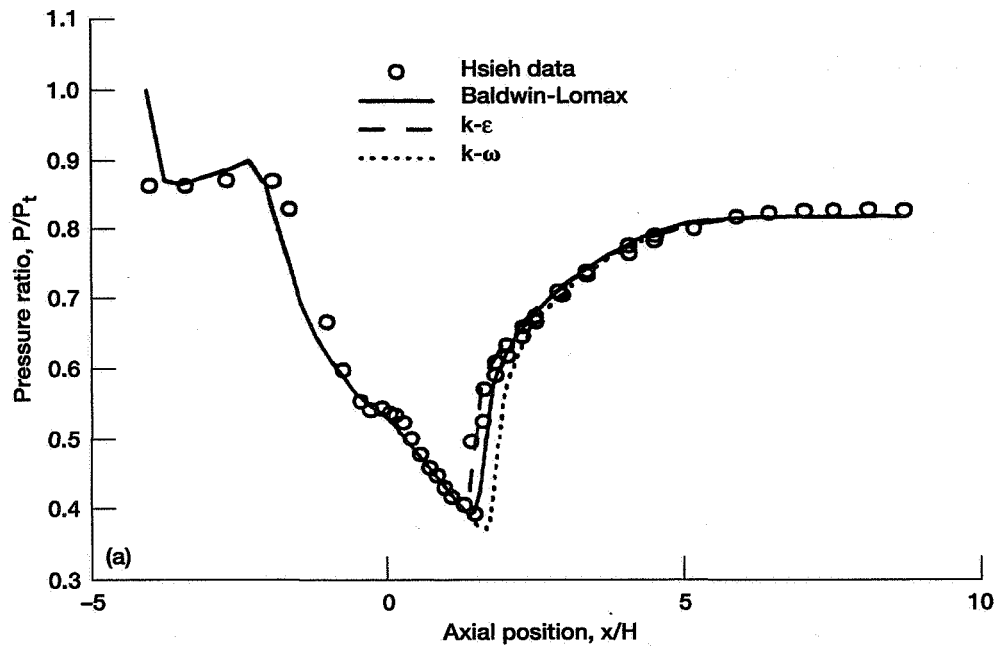


Figure 11.—Pressure distributions for Sajben diffuser (weak shock). (a) Top surface.  
(b) Bottom surface.

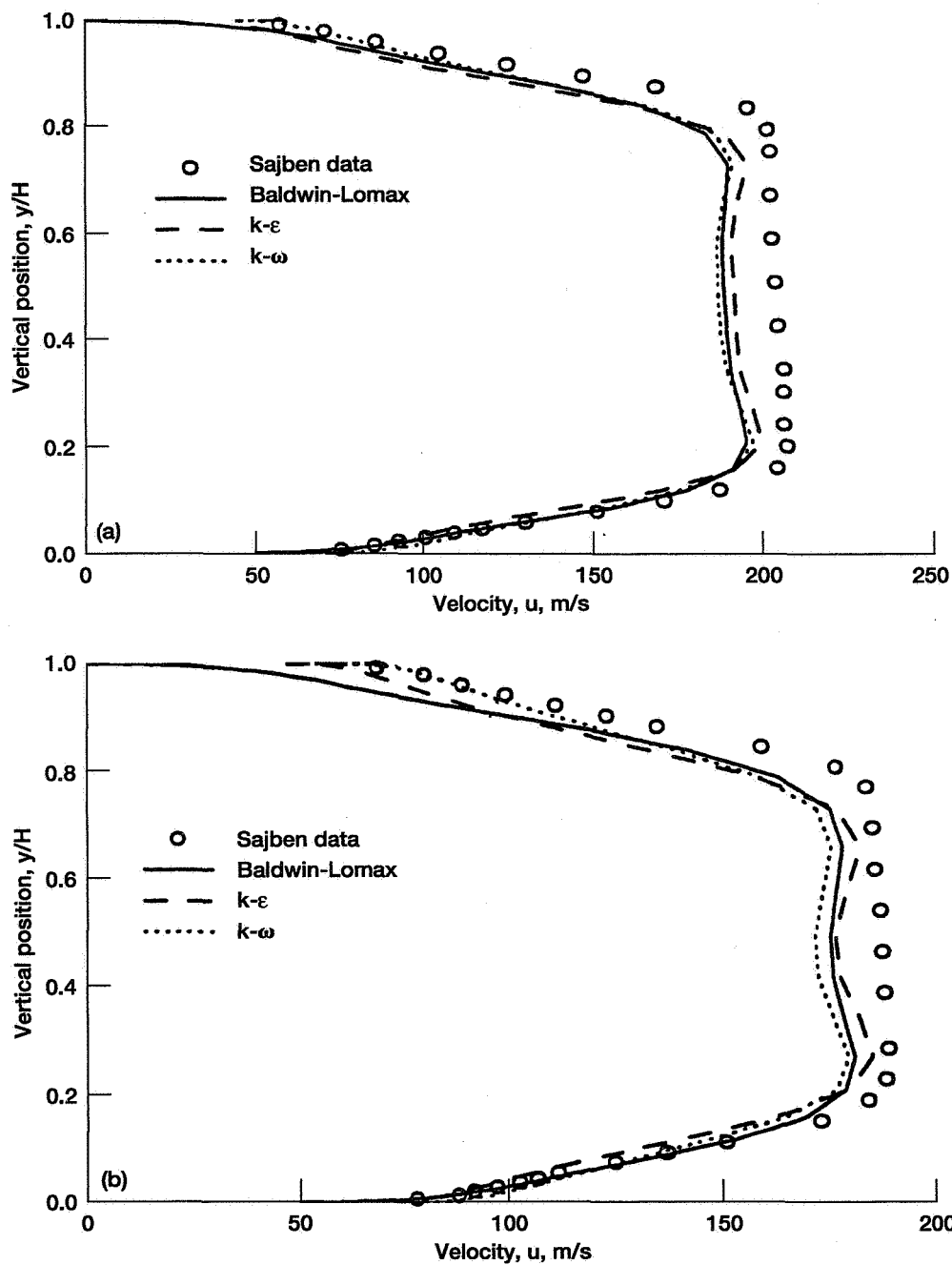


Figure 12.—Sajben diffuser velocity profiles (weak shock) at two axial positions  $x/H$ .  
 (a)  $x/H = 4.6$ . (b)  $x/H = 6.3$ .

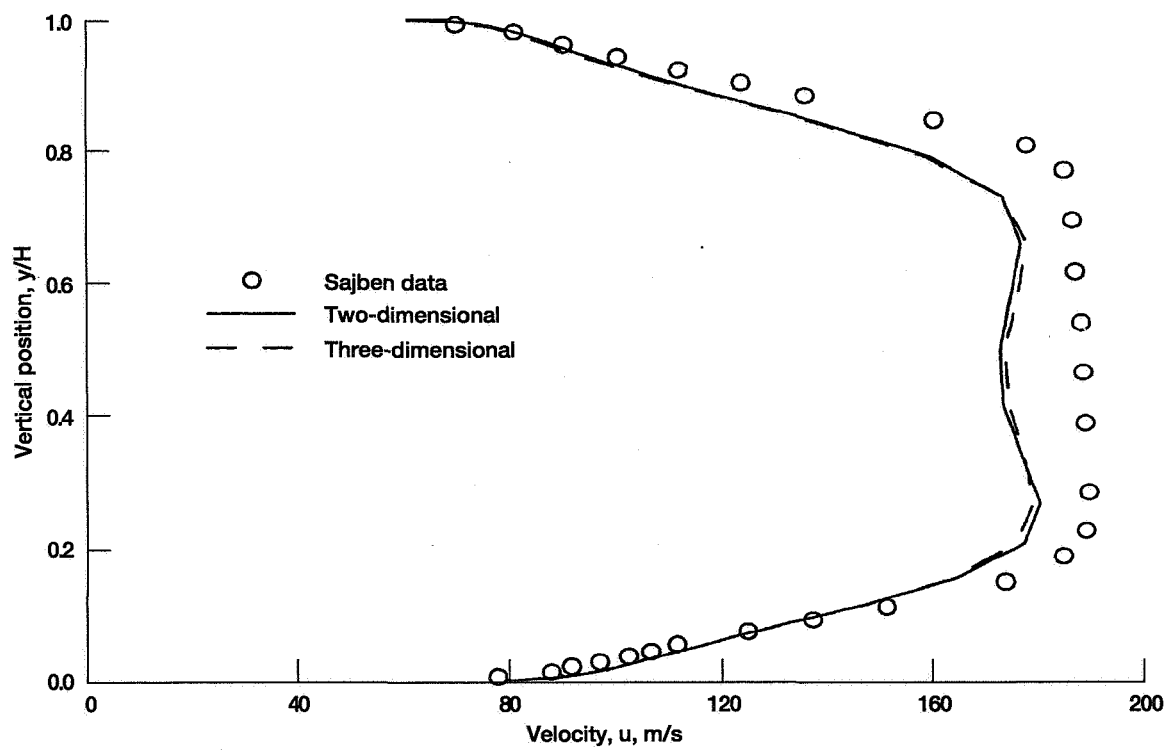


Figure 13.—Comparison of  $k-\omega$  results for Sajben diffuser (weak shock) at axial position  $x/H = 6.3$ .

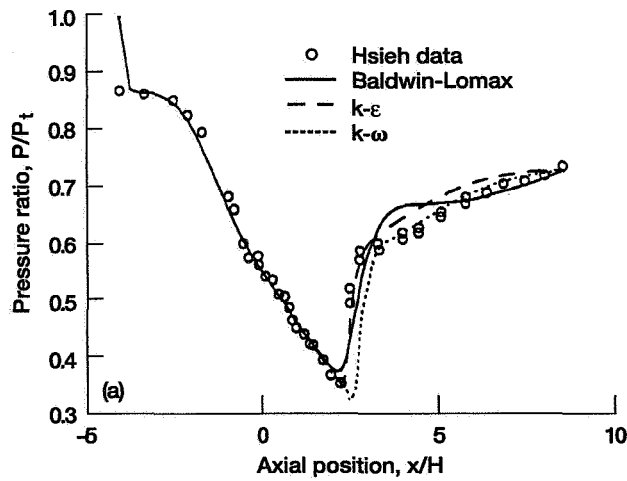
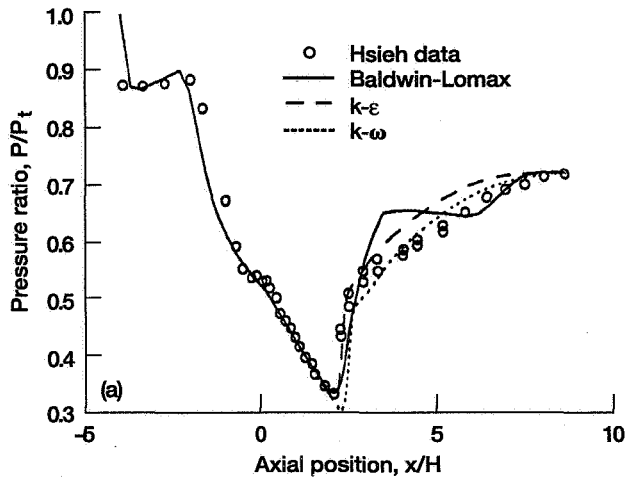


Figure 14.—Pressure distributions for Sajben diffuser (strong shock). (a) Top surface. (b) Bottom surface.

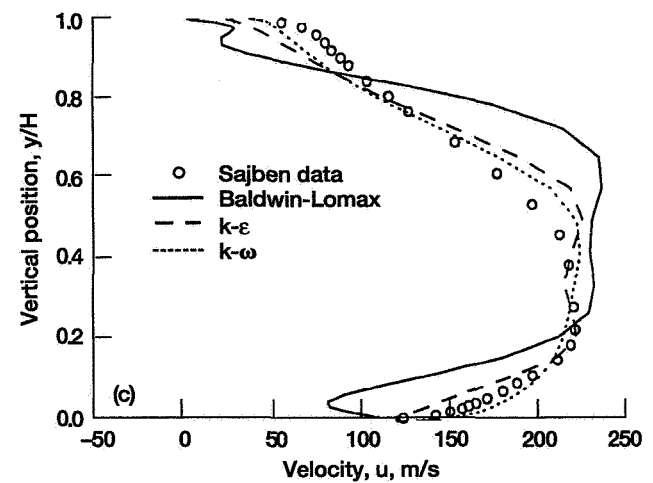
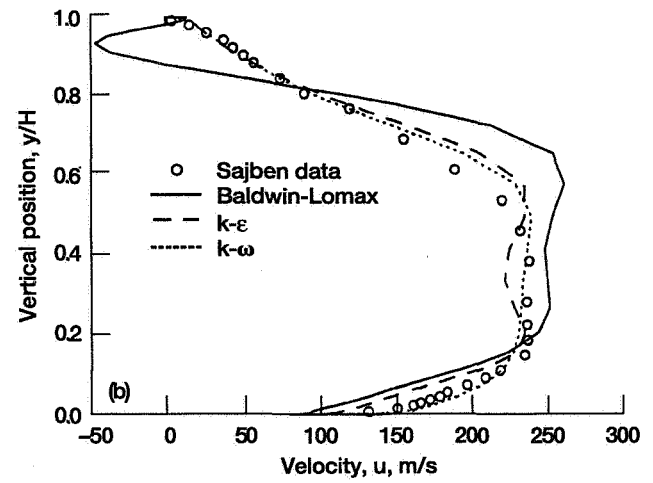
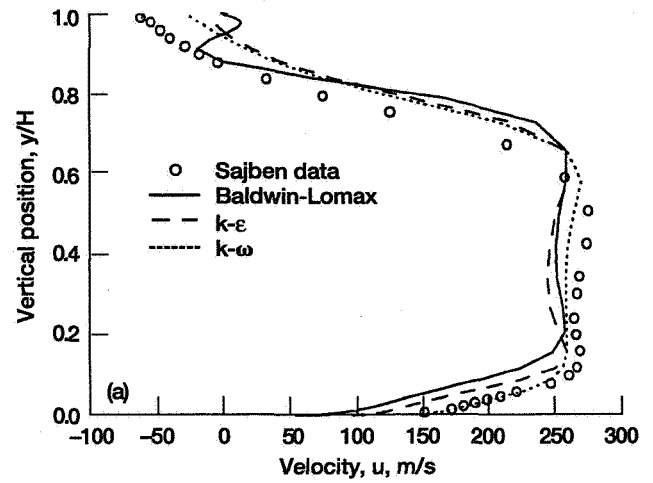


Figure 15.—Sajben diffuser velocity profiles (strong shock) at three axial positions  $x/H$ . (a)  $x/H = 4.6$ . (b)  $x/H = 6.3$ . (c)  $x/H = 7.5$ .

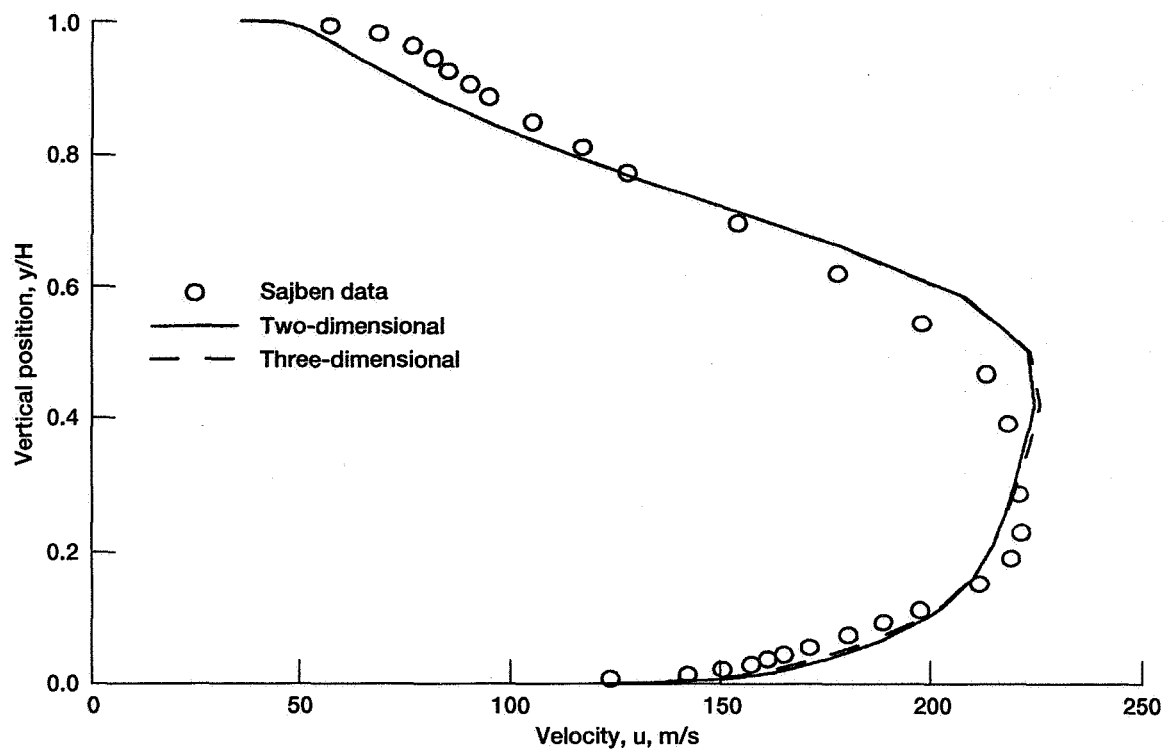


Figure 16.—Comparison of  $k-\omega$  results for Sajben diffuser (strong shock) at axial position  $x/H = 7.5$ .

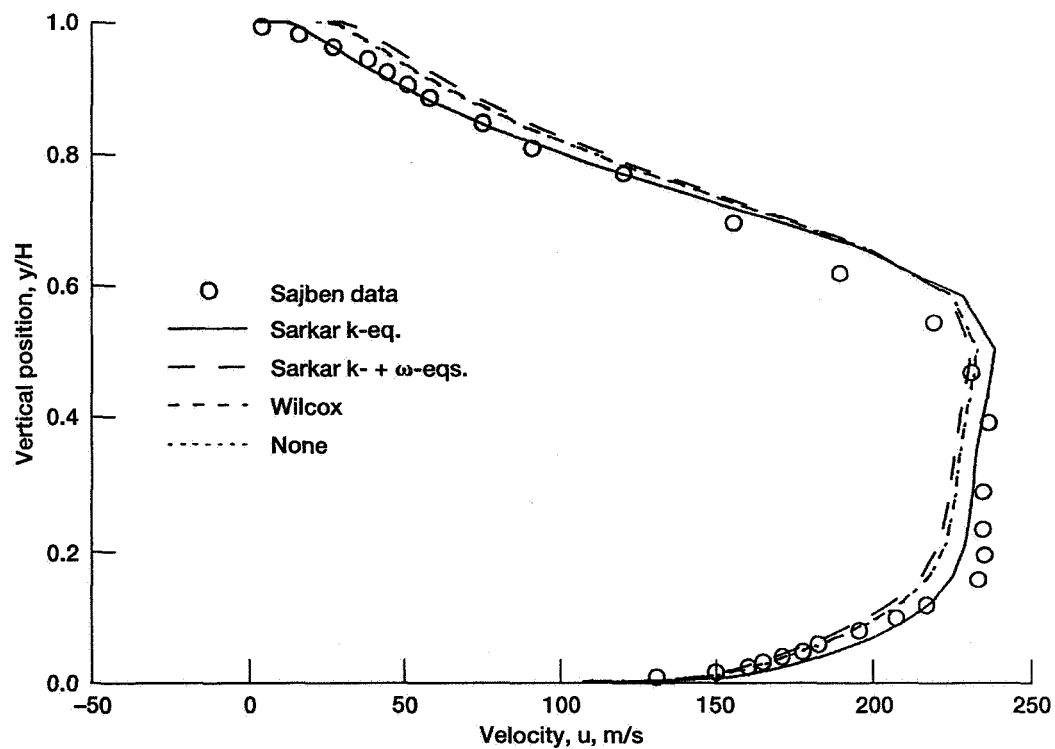


Figure 17.—Comparison of compressibility corrections for Sajben diffuser (strong shock) at axial position  $x/H = 6.3$ .

REPORT DOCUMENTATION PAGE			Form Approved OMB No. 0704-0188	
Public reporting burden for this collection of information is estimated to average 1 hour per response, including the time for reviewing instructions, searching existing data sources, gathering and maintaining the data needed, and completing and reviewing the collection of information. Send comments regarding this burden estimate or any other aspect of this collection of information, including suggestions for reducing this burden, to Washington Headquarters Services, Directorate for Information Operations and Reports, 1215 Jefferson Davis Highway, Suite 1204, Arlington, VA 22202-4302, and to the Office of Management and Budget, Paperwork Reduction Project (0704-0188), Washington, DC 20503.				
1. AGENCY USE ONLY (Leave blank)		2. REPORT DATE April 1996	3. REPORT TYPE AND DATES COVERED Technical Memorandum	
4. TITLE AND SUBTITLE  Implementation of a Two-Equation k- $\omega$ Turbulence Model in NPARC			5. FUNDING NUMBERS  WU-537-02-23	
6. AUTHOR(S)  Dennis A. Yoder, Nicholas J. Georgiadis, and Paul D. Orkwis				
7. PERFORMING ORGANIZATION NAME(S) AND ADDRESS(ES)  National Aeronautics and Space Administration Lewis Research Center Cleveland, Ohio 44135-3191			8. PERFORMING ORGANIZATION REPORT NUMBER  E-9955	
9. SPONSORING/MONITORING AGENCY NAME(S) AND ADDRESS(ES)  National Aeronautics and Space Administration Washington, D.C. 20546-0001			10. SPONSORING/MONITORING AGENCY REPORT NUMBER  NASA TM-107080 AIAA-96-0383	
11. SUPPLEMENTARY NOTES Prepared for the 34th Aerospace Sciences Meeting and Exhibit sponsored by the American Institute of Aeronautics and Astronautics, Reno, Nevada, January 15-18, 1996. Dennis A. Yoder and Nicholas J. Georgiadis, NASA Lewis Research Center; Paul D. Orkwis, University of Cincinnati, Cincinnati, Ohio 45221. Responsible person, Nicholas J. Georgiadis, organization code 2740, (216) 433-3958.				
12a. DISTRIBUTION/AVAILABILITY STATEMENT  Unclassified - Unlimited Subject Category 02  This publication is available from the NASA Center for Aerospace Information, (301) 621-0390.			12b. DISTRIBUTION CODE	
13. ABSTRACT (Maximum 200 words)  The implementation of a two-equation k- $\omega$ turbulence model into the NPARC flow solver is described. Motivation for the selection of this model is given, major code modifications are outlined, new inputs to the code are described, and results are presented for several validation cases: an incompressible flow over a smooth flat plate, a subsonic diffuser flow, and a shock-induced separated flow. Comparison of results with the k- $\epsilon$ model indicate that the k- $\omega$ model predicts simple flows equally well whereas, for adverse pressure gradient flows, the k- $\omega$ model outperforms the other turbulence models in NPARC.				
14. SUBJECT TERMS  NPARC; Turbulence; Boundary layer; Turbulent boundary conditions; Transition; Roughness; Diffuser; Adverse pressure gradient			15. NUMBER OF PAGES 21	
			16. PRICE CODE A03	
17. SECURITY CLASSIFICATION OF REPORT Unclassified	18. SECURITY CLASSIFICATION OF THIS PAGE Unclassified	19. SECURITY CLASSIFICATION OF ABSTRACT Unclassified	20. LIMITATION OF ABSTRACT	